Numerical Computations of Internal Combustion Engine related Transonic and Unsteady Flows

by

Olle Bodin

February 2009
Technical Reports from
Royal Institute of Technology
KTH Mechanics
SE-100 44 Stockholm, Sweden

Akademisk avhandling som med tillstånd av Kungliga Tekniska Högskolan i Stockholm framlägges till offentlig granskning för avläggande av teknologie licentiatexamen fredagen den 2:a Mars 2009 kl 10.15 i sal E31, Lindstedtsvägen 3, Kungliga Tekniska Högskolan, Vallhallavägen 79, Stockholm.

Universitetsservice US–AB, Stockholm 2009

Numerical computations of internal combustion engine related transonic and unsteady flows

Olle Bodin 2009,
KTH Mechanics
SE-100 44 Stockholm, Sweden

Abstract

Vehicles with internal combustion (IC) engines fueled by hydrocarbon compounds have been used for more than 100 years for ground transportation. During the years and in particular in the last decade, the environmental aspects of IC engines have become a major political and research topic. Following this interest, the emissions of pollutants such as NO_x, CO_2 and unburned hydrocarbons (UHC) from IC engines have been reduced considerably.

Yet, there is still a clear need and *possibility* to improve engine efficiency while further reducing emissions of pollutants. The maximum efficiency of IC engines used in passenger cars is no more than 40% and considerably less than that under part load conditions. One way to improve engine efficiency is to utilize the energy of the exhaust gases to turbocharge the engine. While turbocharging is by no means a new concept, its design and integration into the gas exchange system has been of low priority in the power train design process. One expects that the rapidly increasing interest in efficient passenger car engines would mean that the use of turbo technology will become more widespread.

The flow in the IC-engine intake manifold determines the flow in the cylinder prior and during the combustion. Similarly, the flow in the exhaust manifold determines the flow into the turbine, and thereby the efficiency of the turbocharging system.

In order to reduce NO_x emissions, exhaust gas recirculation (EGR) is used. As this process transport exhaust gases into the cylinder, its efficiency is dependent on the gas exchange system in general. The losses in the gas exchange system are also an issue related to engine efficiency. These aspects have been addressed up to now rather superficially. One has been interested in global aspects (e.g. pressure drop, turbine efficiency) under *steady state* conditions.

In this thesis, we focus on the flow in the exhaust port and close to the valve. Since the flow in the port can be transonic, we study first the numerical modeling of such a flow in a more simple geometry, namely a bump placed in a wind tunnel. Large-Eddy Simulations of internal transonic flow have been carried out. The results show that transonic flow in general is very sensitive to small disturbances in the boundary conditions. Flow in the wind tunnel case is always highly unsteady in the transonic flow regime with self excited shock oscillations and associated with that also unsteady boundary-layer separation.

To investigate sensitivity to periodic disturbances the outlet pressure in the wind tunnel case was varied periodically at rather low amplitude. These low amplitude oscillations caused hysteretic behavior in the mean shock position and appearance of shocks of widely different patterns.

The study of a model exhaust port shows that at realistic pressure ratios, the flow is transonic in the exhaust port. Furthermore, two pairs of vortex structures are created downstream of the valve plate by the wake behind the valve stem and by inertial forces and the pressure gradient in the port. These structures dissipate rather quickly. The impact of these structures and the choking effect caused by the shock on realistic IC engine performance remains to be studied in the future.

Descriptors: Transonic flow, Hysteresis, Shock/boundary-layer interaction, Exhaust valve, Large Eddy Simulation.

Preface

This licentiate thesis consist of two parts. The first part gives an overview of transonic internal flows and a short summary of the results. The second part consists of three papers, which are adjusted to comply with the present thesis format for consistency. The content of the papers have been updated and include minor refinements as compared to the published versions. In Chapter **??** of the first part of the thesis the contribution of the respondent to the papers is stated.

February 2009, Stockholm
Olle Bodin

The significant problems we face can not be solved at the same level of thinking we were at when we created them.

Albert Einstein (1879–1955)

Contents

Part I

Overview and summary

CHAPTER 1

Introduction

Vehicles with internal combustion engines fueled by liquid hydrocarbon of some sort has been a significant transport mode for about 100 years. During the later part of the evolution towards present day, the focus of development has steadily moved towards less impact on the environment. Not only are the emissions of pollutants such as NO_x, CO_2 and unburned hydrocarbons reduced, but also acoustic pollution.

An obvious way of decreasing the environmental impact of a vehicle is to reduce the amount of fuel it consumes, increase the efficiency of the vehicle. For reciprocal internal combustion engines, the efficiency with regard to output power versus fuel energy content is typically less than 40%. The main loss sources in the engine are cooling and flow-related.

One way to make an engine more efficient is to use the energy of the exhaust gases to turbocharge it, and thereby reduce the flow losses. While turbocharging is by no means a new concept, the rapidly increasing interest in efficient passenger cars mean that the use of turbo technology will become more widespread.

Even with turbocharging however, much of the exhaust energy is still lost. Between the cylinder and the turbocharger turbine the exhaust gases pass through first the exhaust port containing the exhaust valve, and then the exhaust manifold. Along this path, as much as 30% of the available energy at the exhaust valve is lost, of course depending on the specific engine and operating conditions. Clearly, the gas flow in this part of the engine can have a large impact on the total efficiency of the engine

The work presented here is aimed at deepening the knowledge of the flow in internal combustion engines through detailed simulations of the flow in the exhaust port. More specifically, the transonic flow in a duct with a bump and a simple exhaust port is analyzed. The flow in the exhaust port can be characterized as follows:

- Transonic
- Unsteady
- Transitional and turbulent flow
- Presence of unsteady separation bubbles
- Presence of unsteady and intermittent shocks
- Moving valve boundaries
- Geometrically small

The approach taken in this work is to use the more geometrically simple example of internal and transonic flow over a bump to evaluate the analysis of the complicated flow phenomena found in unsteady transonic flows. For this geometry, experimental data is available making it possible to evaluate the computational results by comparison to the experiments. As a second step, we have allowed unsteadiness in the flow conditions by varying the outlet static pressure. The results show clearly the intricate character of transonic flows; namely, the presence of time-varying complex shock systems and that the flow conditions under a given state of boundary conditions (BC) depends on flow history (i.e. the flow is hysteretic). Additionally, one encounters unsteady turbulent flow noting separated boundary layers with time dependent location and extent. The knowledge, analysis, and basic understanding together with similar methodology from the bump flow investigation is then used to investigate the transonic and unsteady flow in a model internal combustion engine exhaust port. The port geometry has a significantly more complex geometry resulting in new flow features that are not found in the case of the bump. Features are secondary flow due to centrifugal instability and wake effects behind the valve stem as well as their interaction.

The unsteadiness of the shock in the transonic bump flow is a result of the interaction between the separating boundary layer and the shock. Acoustic disturbances in the flow are present but is not significantly affecting the dynamics of the shock motion. The shock position exhibit hysteresis when subjected to slowly varying outlet pressure because of varying shock Mach number in accelerating and decelerating flow. For the exhaust port, two distinctive pairs of vortices are generated downstream of the valve by centrifugal instabilities in the port and by the wake behind the valve. These secondary flow structures are quite strong initially and, depending on the conditions downstream of the valve, are convected downstream in a more or less coherent fashion.

The two first papers consider the wind tunnel geometry, while the third consider the flow in a model exhaust port.

CHAPTER 2

Transonic flows

The *compressibility* of a fluid flow has a potentially large impact on the flow behavior and flows of gases are in general *compressible*, i.e. has compressible effects. However, when the propagation speed of sound in the fluid is large compared to the fluid speed, the compressibility of the fluid is low and pressure perturbations propagate in all directions with high speed. Because of this, it is relevant to quantify when the speed of sound is "high". This can be done through the Mach number,

$$Ma = \frac{U_{inf}}{a}, \tag{2.1}$$

where U_{inf} is the speed of the fluid and a is the speed of sound in the fluid.

Two easily defined Mach numbers have special significance. First, the limiting case of $Ma = 0$ is termed as the *incompressible* limit. For this case it has to be stressed that the incompressible limit differs in essence from low speed compressible flow, i.e. when the Mach number is small but not zero.

This is so because, in terms of losses, the effects of compressibility behaves as the square of the Mach number. Thus, for engineering purposes and from a numerical point of view, flows with Mach number lower than about $0.3 - 0.4$ behaves as incompressible flows. Although the exact dividing value is not easily defined, most agree that a maximum Mach number above 0.3 signify that the flow in question has significant compressible effects and is *compressible*.

The other limiting case is when the Mach number is unity, i.e. when the flow is *sonic*. For this case, the acoustic waves propagate at the same speed as the flow. For $Ma > 1$ the flow is termed *supersonic* because the flow speed exceeds the speed of sound and hence, no sound wave can propagate upstream. Flows that contain significant sub-, and supersonic regions, are called *transonic*.

Transonic flow is present in many engineering applications and in IC engine related flows. For example, the flow may be transonic past the intake and exhaust valves and in the turbocharger (both compressor and turbine). The shocks that occur imply a (near) discontinuity in some of the flow variables such as density, pressure and shock normal velocity.

The flow may separate if the pressure gradient is not favorable enough. This also happens at strong variations in the shape of the wall or due to a

shock, which implies a steep pressure increase. The shocks in the transonic flow regime tend to be unsteady, leading to unsteady flow separation. These effects imply non-recoverable losses and fluctuating forces induced by the flow.

Transonic flows are in general sensitive to boundary conditions (geometrical or flow conditions). This sensitivity is even more pronounced for internal flows where shocks may interact with wall boundary layers due to shock reflections and unsteady boundary layer separation. The strong coupling between non-linear phenomena, shock shape and unsteady boundary layers, is the basic reason for the complexity of the flow. The complexity of transonic flow stems not only from the non-linear interaction but also from the formation of multiple-states which leads to hysteresis.

An experimental investigation by Liu & Squire (1988) considers the effect of a bump curvature and pressure ratio on the flow structure in transonic tunnel flow. The investigators use circular-arc bumps of varying radii under different driving pressure, such that the shock Mach number is in the range between 1 and 1.82. In this range one finds both weak and strong shocks, as well as flows with and without flow separation.

Three distinct types of boundary layer behavior have been observed: *(i)* fully attached flow, *(ii)* trailing edge separation, where the flow separates due to the adverse pressure gradient caused by the geometrical shape of the wall and, *(iii)* shock-induced separation, where the separation occurs behind the shock foot. The pressure increase over the shock may be substantial when the shock-normal Mach number upstream of the shock is not very close to unity. Thus, shocks often induce adverse pressure gradients that lead to a thickening of the boundary layer. Such a thickening leads to a sharper change in the flow direction, which leads to an even stronger shock and hence, even stronger flow separation. Thus, it is easy to come to the conclusion that such flows are inherently unstable even for small perturbations.

The study of Liu & Squire (1988) shows that there exist a critical Mach number, Ma_c, where the separation changes type from trailing-edge to shock-induced and that this Mach number has the most extensive separation in the Mach number range under consideration for all bump curvatures.

The general flow structure was found to depend on the pressure ratio so that at a low ratio the shock first forms as a normal shock at the bump surface and as the pressure ratio increases it gradually moves downstream and becomes stronger. With further increase in the pressure ratio the shock extends over the whole tunnel, reaching the top wall of the tunnel where it is reflected. With even higher pressure ratio, the shock bifurcates, forms a λ-shock and the reflected shock may be either a regular- or a Mach-reflection depending on the incipient shock angle. The curvature of the bump effects the flow by increasing the shock strength with increasing curvature while for the smallest

curvatures, the flow did not form a λ-shock at all. The critical Mach number was found to be nearly independent of the curvature of the circular arc bump ($Ma_c = 1.3$). If this Mach number is exceeded, the separation of the boundary layer is always shock-induced. The goal of the study of Liu & Squire (1988) was not to investigate the dynamics of the shock. However, indications of shock oscillations were found in the results.

2.1. Shock theory

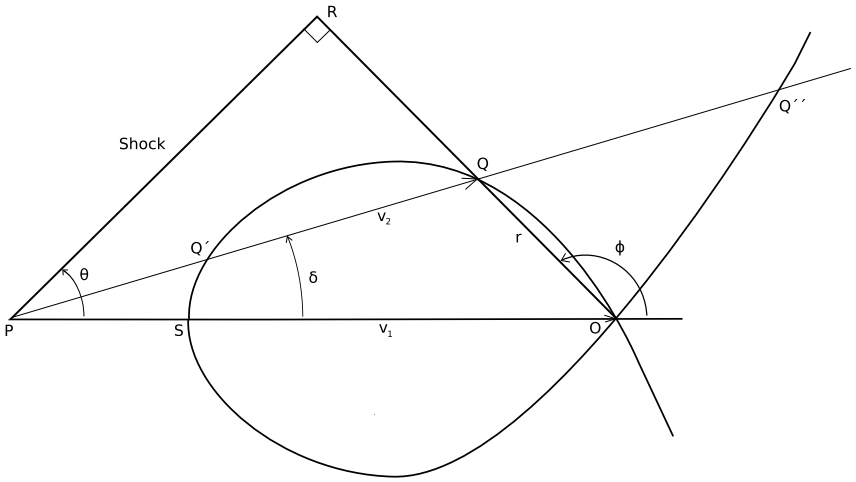

FIGURE 2.1. Oblique shock with shock polar.

Shocks are classified as either normal or oblique referring to their angle with respect to the incoming flow. As all shocks considered in this work are oblique, most of the discussion and background will concern oblique shocks of which normal shocks are a special case. While normal shocks can be described in one dimension, oblique shocks are by their nature two or three-dimensional.

Oblique shocks occur when a supersonic flow is redirected by for example a change in geometry such as a compression corner or a bump. The response of the flow is to change the direction of the stream lines as they pass through the oblique shock in order to accommodate the geometry change. Most textbooks that cover compressible flow , for example Anderson (2003), will contain

derivations of the oblique shock relations so only the resulting relations will be presented here.

In all equations in this section, subscript 1 and 2 denote conditions pre- and post-shock, respectively. The relation between the shock angle θ, and streamline deflection angle δ as a function of incoming Mach number M_1 and $\gamma = c_p/c_v$, the ratio of specific heats, is:

$$\tan(\delta) = 2\cot(\theta) = \left[\frac{M_1^2\sin^2(\theta) - 1}{M_1^2(\gamma + \cos(2\theta)) + 2}\right]. \tag{2.2}$$

One quite interesting property of oblique shocks is that the tangential velocity component is preserved as the streamline passes trough the shock. Now, knowing this and the incoming flow velocity, one may calculate the normal component of the post-shock velocity with the help of equation (2.2).

The geometrical nature of the oblique shock relations allow creative graphical representations, one of which is the so called shock polar. This way of presenting the relations is best considered in a polar coordinate system where:

$$r(\phi) = \left[\frac{2v_1}{(\gamma+1)}\right]\left[\frac{1}{M_1^2\cos(\phi)} - \cos(\phi)\right]. \tag{2.3}$$

The formulation in equation (2.3) was found in Lee (1969) and is represented graphically in figure (2.1), where $r(\phi)$ is the distance between O and Q, as a strophoid-like curve together with the oblique shock. Oblique shocks may be either *weak* or *strong*, depending on weather the flow velocity downstream of the shock is supersonic (weak) or subsonic (strong). The intersections Q and Q' represent the weak and strong shock solutions, respectively, while Q'' represent the so called unphysical shock solution, see Lee (1969). The point S represent the normal shock solution while O is a Mach line or an infinitely weak oblique shock. Velocities pre- and post-shock are represented by the lengths of v_1 and v_2, where the latter can have different lengths depending on shock type. Shock angle and streamline deflection angle are defined by the same letters as in equation (2.2).

2.2. Shock reflections

In the vicinity of walls shocks are reflected. The reflection of an oblique shock can take place in two forms, either as a regular reflection (RR) or as a Mach reflection (MR). An illustration of the two different reflection types can be seen in figure (2.2) where the fluid flow is from left to right and i, r and s mark the incipient shock, the reflected shock and the Mach stem, respectively. When the flow encounters the wedge, a shock is formed with an incipient angle that is dependent on both the incoming Mach number and the wedge angle.

If the flow Mach number increases from a state where the reflection is a RR, the angle will become smaller and the reflection will eventually transition

from RR to MR. If the process is reversed and the incoming Mach number is reduced from a state where the reflection is a MR, the RR does not occur at the same incoming Mach number as the RR-MR transition (Hornung & Taylor 1982; Hornung & Robinson 1982; Ben-Dor *et al.* 2002; Ben-Dor 1999). This

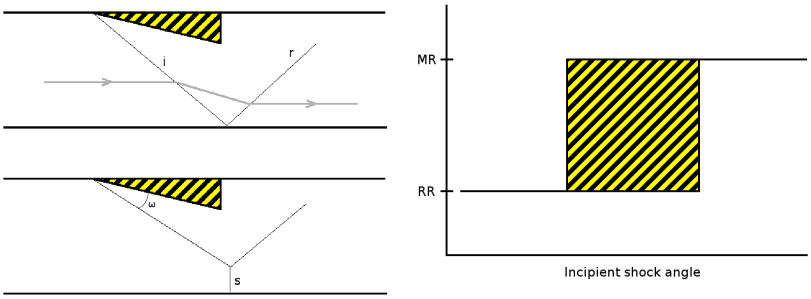

FIGURE 2.2. Left: Defining regular reflection (top), and Mach reflection (bottom). Right: Illustrating the hysteresis in the transition between Mach- and regular-reflection.

transition hysteresis is qualitatively illustrated in figure (2.2), where the angle increases from left to right. The marked area in figure (2.2) is called the *dual domain* due to the possibility of having either RR or MR in this range of shock angles. The dual domain is bounded by two angles, ω_{RR} and ω_{MR}, beyond which only one type of reflection is possible.

It turns out that the RR-MR transition is sensitive to disturbances so that in practice, the transition usually happens beyond ω_{RR} but before ω_{MR} while MR-RR transition usually occurs at ω_{RR}. However, it must be stressed that both reflections are stable and possible anywhere in the dual range although the MR is more insensitive to small disturbances in the hysteretic range.

2.3. Self excited flow

In transonic flows, the shock position is often unsteady (Chen *et al.* 1979; Liu & Squire 1988; Bogar *et al.* 1983). The most common mechanisms behind this are either acoustic interaction, shock/boundary-layer interaction or a combination of both.

The acoustic interaction scenario involve acoustic waves interacting with the shock in a transonic wind tunnel and has been found by Bogar *et al.* (1983) among others. Bogar *et al.* (1983) reports that this phenomenon occurs when the shock Mach number was low enough such that the flow remains unseparated. The mechanism of the shock motion for this flow could then be described using (linear and one-dimensional) acoustic theory.

For stronger shocks, when the flow may have a separated boundary layer, this type of mechanism could not be found and the authors suggest that the unsteadiness is related instead to convective effects in the boundary layer or some other dynamics of the separated boundary layer. These findings are confirmed and expanded in a paper by Salmon *et al.* (1983) where it is stated that acoustic perturbations exist in both the strong and weak shock case but that these are overwhelmed by perturbations caused by the boundary layer in the strong shock case.

The type of unsteadiness depends on the shock Mach number and the geometry of the flow. Chen *et al.* (1979) have found that for weak shocks (where the boundary layer separation is caused by the adverse pressure gradient) the shock oscillation frequency decreases with increasing shock strength. For strong shocks, when the separation is caused by the shock, the oscillation frequency and its amplitude increase with increasing shock strength (or shock Mach number). The authors also postulate a one-dimensional model where the main dynamics of the separated region can be viewed as two wave-like families moving up, and downstream, respectively. The upstream waves are fast and weak, while downstream waves are slow and strong. This model is supported by space-time correlations which show that there are two distinct types of perturbations that are correlated to the shock motion. One of these are propagating upstream and dominate at small pressure ratios while the other is convected downstream in the boundary layer and becomes dominant as the pressure ratio increases. The proposed model agrees well with the space-time correlation results presented in the paper.

As the flow passes the shock there is a strong deceleration, primarily in the streamwise component of the velocity. This causes a strong increase in the streamwise velocity fluctuations and a large increase in the turbulence production at the shock which is further enhanced when the flow separates. Due to this strong perturbation, the properties of the incoming boundary layer upstream of the shock will have negligible influence on the free shear layer of the separation, see Délery (1983).

2.4. Forced flow

Due to the unsteady behavior of the shock, it is natural to investigate the behavior of the system when it is subjected to periodic perturbations. The possibility of controlling the shock motion and strength by careful choice of the perturbations can be an important tool in certain applications. One may apply the knowledge of such behavior to for example transonic wings, where the fluctuating forces may cause structural problems, decrease the efficiency of the wing or cause excessive noise.

Many investigations of periodic forcing in bump flow exist, for example Galli *et al.* (2005) where the outlet pressure in the transonic wind tunnel was perturbed by a rotating elliptical shaft to create a sinusoidal-like variation in the pressure downstream of the bump. Because the shock position was highly dependent on the outlet pressure a disturbance of the natural oscillation of the shock is created. Galli *et al.* (2005) found that damping the shock oscillations was possible by the appropriate choice of perturbation frequency, but did not report any attempts at amplifying it. Furthermore, Galli *et al.* (2005) found that the shock oscillation amplitude is inversely dependent on the perturbation frequency so that an increase in frequency leads to a decrease in amplitude.

In an investigation by Salmon *et al.* (1983) forcing was induced by a rotating device set into the tunnel wall at a frequency 38% above the frequency corresponding to the peak amplitude in the shock displacement spectra. The results and conclusions of the work by Salmon *et al.* (1983) was that no direct coupling between the natural oscillation of the shock and the forced perturbation could be observed. It was suggested that this could be explained by the broadband nature of the shock oscillation compared to the tonal nature of the perturbation. The authors also stress that the reason for the natural oscillations in the case of strong shocks and shock-induced separation is boundary layer perturbations. Furthermore, that transverse (normal to the boundary layer) propagation of these perturbations is an important part of the mechanism behind the natural oscillations of the strong shock.

An extensive investigation of forced flow by periodic perturbations in the same geometry and facility as Salmon *et al.* (1983) was conducted by Sajben *et al.* (1984). In this investigation the same forcing method as in Salmon *et al.* (1983) was used but, with a much wider frequency range, including the natural frequency of the shock oscillation. Just like Salmon *et al.* (1983) and Bogar *et al.* (1983), two distinct flow configurations corresponding to weak and strong shocks were found.

For weak shocks, the natural shock oscillation spectra has two peaks. One of these correspond to the acoustic interaction between the shock and the outflow boundary that can be described by streamwise propagation of plane waves. The other peak is explained through the perturbations that are created in the unseparated boundary layer when subjected to an adverse pressure gradient. The natural shock oscillation in the case of strong shocks is believed to be caused by turbulence which excite perturbations that propagate both in the core flow and in the boundary layers. Only one peak is present in the shock spectra for the strong shock case and the acoustic interaction peak is not evident although the flow likely contain plane acoustic waves propagating back and fourth in the main flow direction. These acoustic modes are weak and their trace can hardly be observed in the otherwise turbulent flow.

Sajben *et al.* (1984) use one-dimensional acoustic theory to predict the motion of the shock. This simple model gives quite accurate results for the weak-shock case but fails completely to predict the strong shock case. The failure of the one-dimensional approach is the result of neglecting the boundary layer and other viscous effects.

The investigation by Sajben *et al.* (1984) failed to excite any resonant behavior in the shock oscillation in the weak and strong shock cases. The proposed explanation for this is that the modes responsible for the natural oscillation is not exited by the forced perturbations, which are close to plane waves propagating along the length of the diffuser. This explanation is most logical for the strong shock case, where there was no peak in the shock motion spectra associated with acoustic modes. For the weak shock case, the peak in the shock motion spectra associated with acoustics is not the main mode. The diffuser geometry is described as two-dimensional, having a two-parameter set of natural modes in a strict acoustic sense. Furthermore, the presence of the boundary layer, especially in the strong shock case, is likely to increase the number of modes even further. The exact mode that is responsible for the natural shock oscillation has not been identified but the conclusion is that the plane acoustic waves are not a likely candidate as the driving mechanism for either case.

The reflective properties of the shock with respect to velocity and pressure perturbations is important as it determines the upstream boundary condition when the flow is choked. The downstream boundary in both experiments and simulations is often more or less reflective and in the case of perturbed flow, is also the source of the perturbations. Sajben *et al.* (1984) found that the reflective properties of the shock is dependent on the property considered, flow properties and weather or not a forced perturbation is present in the flow. Depending on these, the reflection can vary between an almost total reflection in a "closed end" fashion, a reflection coefficient of 1, and zero. As many other properties of shocks, the reflective behavior can not be easily explained, or modeled, for other than weak shocks and pressures perturbations. Strong shocks and their strong coupling to boundary layer dynamics make the reflective properties difficult to quantify.

2.4.1. *Hysteresis*

Hysteresis may occur in any non-linear system and implies that a system can attain a distinct number of states depending on the path taken to get to the state. The non-linearity of the Navier-Stokes and the Euler equations imply the possibility of hysteresis both for viscous and inviscid flows.

An example not directly related to the present work is the stall characteristics of certain airfoils where the stall angle does not coincide with the angle of

boundary layer reattachment. In the transition between regular reflection and Mach reflection, hysteresis can be observed because of the existence of the dual domain where both reflections are possible. The transition angle is dependent on the path to it (c.f. Ben-Dor *et al.* (2002)).

Another example of hysteresis in transonic flows is the mean position of the shock in bump flow with steady state boundary conditions, but possibly with different initial conditions. Such behavior has been reported by Moroianu *et al.* (2005) and also by us (Chapter (4) and Papers (1) and (2)). In these investigations, hysteresis in the shock position is observed when very low-frequency perturbations are applied while keeping the flow in the quasi-steady regime.

2.5. Losses in transonic flows

Aside from the high flow velocity, which by itself serves to increase flow losses due to the dependence of the wall shear stress on the wall-normal velocity gradient, transonic flows have shocks that are associated with additional losses. Here, the example of a normal shock in one-dimensional flow is used to illustrate the concept (Anderson 2003) and, while this is a much simplified case, the principles can be expected to hold true also for more complex and practical cases where shocks occur. For this flow case the following equations are valid and describe the ratio of the temperature and pressure before and after the shock as function of the flow Mach number before the shock:

$$\frac{p_2}{p_1} = 1 + \frac{2\gamma}{\gamma+1}(M_1^2 - 1), \tag{2.4}$$

$$\frac{T_2}{T_1} = \frac{h_2}{h_1} = \left[1 + \frac{2\gamma}{\gamma+1}(M_1^2 - 1)\right]\left[\frac{2 + (\gamma-1)M_1^2}{(\gamma+1)M_1^2}\right]. \tag{2.5}$$

Now, consider the second law of thermodynamics in the following form:

$$s_2 - s_1 = c_p \ln\left(\frac{T_2}{T_1}\right) - R \cdot \ln\left(\frac{p_2}{p_1}\right). \tag{2.6}$$

Equation (2.6) gives the change in entropy as a function of the change of temperature and pressure. This relation can be used together with equations (2.4) and (2.5) to show that the change in entropy over a normal shock is a function of the square of the Mach number upstream to the shock,

$$s_2 - s_1 = c_p \ln\left(\left[1 + \frac{2\gamma}{\gamma+1}(M_1^2 - 1)\right]\left[\frac{2 + (\gamma-1)M_1^2}{(\gamma+1)M_1^2}\right]\right) - R \cdot \ln\left[1 + \frac{2\gamma}{\gamma+1}(M_1^2 - 1)\right]. \tag{2.7}$$

It is clear that Equation (2.7) only has physical meaning for $M_1 \geq 1$ as the entropy would otherwise decrease over the shock, something which is not possible.

CHAPTER 3

Turbulent flow modeling and computational aspects

The equations describing fluid flow are the Navier-Stokes equations (NSE) and consist of the conservation of mass (3.1), momentum (3.2) and energy (3.3) together with a relation of state for the fluid (3.4). The equations read:

$$\frac{\partial \rho}{\partial t} + \frac{\partial}{\partial x_j}(\rho \cdot u_j) = 0, \tag{3.1}$$

$$\frac{\partial}{\partial t}(\rho \cdot u_i) + \frac{\partial}{\partial x_j}(\rho \cdot u_i \cdot u_j) = -\frac{\partial p}{\partial x_i} + \frac{\partial \tau_{ij}}{\partial x_j} + \rho f_i, \tag{3.2}$$

$$\frac{\partial}{\partial t}(\rho \cdot h) + \frac{\partial}{\partial x_j}(\rho \cdot u_j \cdot h) = \frac{\partial p}{\partial t} + u_j \frac{\partial p}{\partial x_j} + \tau_{ij}\frac{\partial u_i}{\partial x_j} - \frac{\partial q_j}{\partial x_j} + W_{ext} + q_H, \tag{3.3}$$

$$p = n \cdot R \cdot \rho \cdot \ T. \tag{3.4}$$

Above, ρ is the density, p the pressure, T the temperature, x_i the cartesian coordinates, t the time, u_i, i=1,3 is the velocity vector, f_i an external force field, τ_{ij} is the viscous shear stress tensor, h is the specific enthalpy, R is the gas constant and q_i is the heat flux. W_{ext} is the work of external volume forces and q_H is an external heat source. The heat flux q_i is modeled through Fourier's law.

The viscous shear stress tensor, τ_{ij} is for a Newtonian fluid:

$$\tau_{ij} = \mu\left(\frac{\partial u_i}{\partial x_j} + \frac{\partial u_j}{\partial x_i} - \frac{2}{3}\delta_{ij}\frac{\partial u_k}{\partial x_k}\right), \tag{3.5}$$

where μ is the dynamic viscosity of the fluid.

3.1. Turbulence

The flow at very low speeds is linear (and laminar) in character. As the speed increases, the importance of non-linear effects increase as well. The importance of non-linearity can be measured by the ratio of an estimate of the sizes of the

non-linear term to the linear (viscous) term in the momentum equation. This ratio becomes the Reynolds number,

$$Re = \frac{\rho U L}{\mu}, \tag{3.6}$$

where U is a characteristic velocity and L is a characteristic length. Thus, at small Re the flow is linear whereas, for large Re it is not. Non-linear effects may manifest themselves in different ways in the fluid and all are not turbulence. As discussed in the previous chapter, non-linearity may give rise to bifurcating solution (states) and hysteresis. Such effects are deterministic and must be distinguished from the notion of turbulence, it being chaotic in nature.

Turbulence can be described as a three-dimensional and time dependent interacting set of vortices with a range of scales from large ones, related to the global flow (L, T), to small ones, at the so called Kolmogorov length and timescales (ν_k, t_k). Closely linked with this is the so called *energy cascade*, where kinetic energy on average is transferred from the largest eddies (scales) to the smallest, where it is dissipated and turned into heat.

The large scales in a flow are governed, and limited, by the geometry of the problem and are hence not universal. The smallest scales however, for large enough Reynolds numbers, have universal behavior and hence lend themselves for modeling. The Reynolds number, equation (3.6), is also a measure of the separation of these scales and in some sense the character of the turbulence. assumption The kinetic energy of the turbulent flow structures is generated at the large scales by the shear in the mean flow and *on average* the energy is transferred to smaller and smaller scales. However, energy is intermittently transferred in the other direction as well, a process which is commonly called *backscatter*.

An important property of turbulent flows is their enhanced transport and mixing as compared to laminar flows. Increased transport of heat and species may be beneficial in certain applications while it may be undesired in others. For example, aircraft wings can be designed for laminar flow because of the reduced drag at cruise conditions. A turbulent flow over a wing can be beneficial tough, when an attached laminar flow is not possible, for example at high angle of attack when high-lift is required such as at landing and takeoff. Here, the rapid mixing of momentum in the boundary layer of the wing may eliminate the separation of the boundary layer and thereby wing stall.

3.2. Turbulence modeling

The NSE can, in principle, be solved numerically for all speeds and geometries. To do this, one need only to resolve the temporal and spatial scales of the flow. Thus, it is essential to estimate these scales, either a priori or a posteriori. A rough estimate can be made through the Reynolds number, equation (3.6).

The ratio between the smallest (Kolmogorov) scales and the largest (integral) one goes, for very large Re, as $Re^{-3/4}$, whereas the corresponding ratio for the time scales goes as $Re^{-1/2}$. Thus, for a high Re, three-dimensional, turbulent flow one has to carry out computations that grow almost as Re^4. This makes such a direct approach (called Direct Numerical Simulation, DNS) limited to relatively small Re. For most engineering applications DNS cannot be carried out and one has to rely on a model to fill out the gap resulting from the lack of resolution. In contrast to numerical methodologies for the NSE, the state of art of turbulence modeling is much less mature.

Turbulence is normally characterized by statistical properties such as mean, RMS, higher statistical moments, pdf and spectra. Thus, it is natural to work with variables that express directly these statistical quantities. In contrast, DNS provides the instantaneous field which has to be processed in order to determine the statistical properties of the turbulent field.

Equations for the mean of the original variables can be derived easily by averaging the basic equations and writing the instantaneous variables in terms of the mean and a fluctuating component.

The averaging process leads to a system of PDE that resembles the NSE but, has the addition of terms containing correlations of the fluctuating components because of the non-linearity of the NSE, the so called Reynolds Averaged Navier Stokes (RANS) equations. The above mentioned term cannot be expressed in terms of the mean variables and therefore, in order to close the system, one has to express these terms as *functions* of the mean variables (and derivatives of these). This difficulty is called the *closure problem* and the different expressions used to resolve the closure problem lead to different turbulence models. In the following sections we give a very short account to some modeling approaches, with the aim of explaining why in this work we find it appropriate not to use RANS but rather rely on Large Eddy Simulations (LES).

Common turbulence models belong to one of the following categories:

- Direct Numerical Simulation (DNS)
- Large Eddy Simulation (LES)
- Reynolds Averaged Navier-Stokes (RANS)

Beyond this classification, there are also the hybrid approaches where LES and RANS are combined in various ways.

3.2.1. *Direct Numerical Simulation*

Direct numerical simulation resolve all turbulent length scales present in the flow and thereby this approach is in fact not a model! However, as stated above DNS requires such a resolution that it is not applicable for most engineering flows due to the required computational resources.

3.2.2. *Large Eddy simulation*

If the scale content of a flow is not too wide (i.e. relatively low Re), DNS is applicable. For larger Re new small scales are added and, if the energy content of these scales is small, one may still use the same approach as in DNS but refrain from resolving the smallest scales. In fact one may show that the contribution of the small scales vanishes as the square of their amplitude. However, with increasing Re and increasing range of unresolved scales the error committed by the under-resolved DNS becomes larger and the results may be too erroneous.

The basic idea to use not fully resolved DNS may be complimented by some model that accounts for the effects of the unresolved scales on the resolved ones. This is the essence of Large Eddy Simulation (LES); namely to resolve the energetic scales of the flow and model the effect of the unresolved scales on the resolved ones.

In order to illustrate the LES concept, consider a generic transport equation,

$$\frac{\partial u}{\partial t} + \frac{\partial F(x)}{\partial x} = 0. \tag{3.7}$$

Since we cannot resolve all the Fourier components of the solution, but only the larger ones, we simply filter out the higher frequency modes. This can be done by defining the filtering operator as a convolution of a kernel with the variable (integrating over the whole volume). Normally, the kernel has a compact support (such as the so called box filter), but it may also be unbounded (such as the complete Gaussian kernel). In many LES formulations one does not filter the variables explicitly, but rather works with the filtered equations directly.

When equation (3.7) is filtered by applying a (linear) filtering operator on each term, the equation for the filtered variable takes on the form of equation (3.8). Filtering can be done explicitly or implicitly, but the result outcome is similar, i.e. the elimination of the unresolved scales.

$$\frac{\partial \overline{u}}{\partial t} + \frac{\partial F(\overline{x})}{\partial x} = \mathcal{G}. \tag{3.8}$$

The form of $\mathcal{G}$ is dependent on the applied filtering kernel and the filtering operation is assumed to commute with the differentiation. This assumption about commutativity, though correct in the differential form, may not be correct for the discrete counterpart. If the assumption is valid, $\mathcal{G}$ contain terms that stem from nonlinearities in the equation and expresses the effect of the unresolved scales on the resolved ones.

For the Navier-Stokes equations, the only contribution is thus due to the convective terms. The contribution of these terms is called the Sub-Grid Scale

(SGS) term and their effect on the resolved scales has to be accounted for in terms of the resolved scales. The resulting equation system is closed with an SGS model and, given appropriate boundary conditions, it can be solved numerically.

3.2.2a. *Subgrid scale modeling.* The filtering operation in LES creates the SGS terms in the equations, as described above. Due to the importance of the unresolved scales many different approaches to capturing their effect on the resolved scales exist.

Generally speaking, the main role of the SGS term is to account for the effects of the small scales on the large ones and the flow in general. An obvious effect is the dissipation which takes place at the smallest scales of the flow. Thus, SGS terms (and its models) must be *dissipative* which incidentally is also a requirement for stable numerical schemes. Another role that one often associates with the SGS term is that it should have the ability to intermittently transfer energy from small to large scales, to account for backscatter.

Subgrid scale models range from the quite simple ones, aiming at dissipating energy at a correct rate to the more complex ones, of non-local and/or non-linear character. It is important to emphasize that the choice of a certain SGS model must be based on the physical characteristics of the problem and the ability of the model to account for important features of the specific problem. Thus, there are no generally valid SGS models since flows may differ largely from each other also in the small scale characteristics.

The most simple model in practice is the Smagorinsky model. This is a very commonly used SGS model which also serves as the origin of several more advanced models. The Smagorinsky model, equation 3.9, is an analogy to the RANS variant of the eddy viscosity model.

$$\tau_{ij}^r = -2\nu_r \overline{S}_{ij}, \tag{3.9}$$

$$\nu_r = (C_s\Delta)^2\overline{\mathcal{S}}, \qquad \overline{\mathcal{S}} \equiv \left(2\overline{S}_{ij}\overline{S}_{ij}\right)^{1/2}. \tag{3.10}$$

In the Smagorinsky model, the SGS stress, (τ_{ij}^r), is related to the filtered rate of strain, $\overline{S}_{ij}$, as in equation 3.10. The Smagorinsky constant, C_s, and the filter width, Δ, will effect the transfer of energy from the filtered scales to the residual motions.

In the case of the Smagorinsky model and any other eddy viscosity type models, energy transfer is one-way from the filtered motions to the residual motions and there is thus no backscatter. This SGS model is probably the most common and widely used model, although it it is considered to be too dissipative in general and in particular at low Re, transitional, inhomogeneous flows (c.f. Pope (2000)). The Smagorinsky model states explicitly that the SGS term is of second order in terms of the filter width, or cutoff length, Δ.

This implies that the error committed by the SGS model may be larger than the truncation errors. This may cause problems if simulating laminar and transitional flows.

Another issue related to SGS modeling is handling the near wall behavior, where the behavior of turbulence depends on local, and problem dependent, conditions and is not universal. The near wall modeling has been the subject of many papers but due to the above mentioned property of problem dependence, no generally valid model has been formulated. A common approach has been to use models that are in direct analogy to RANS near wall models, such as the van Driest damping function. Another approach that gained some popularity is the hybrid method in which RANS models are used near the wall and LES is used elsewhere.

The hybrid approach is rather straight forward from a conceptual point of view but it may be intricate to implement without causing obviously incorrect velocity profiles. Additionally, there is no solid physical foundation for the hybrid approach since the near wall RANS handling, as is noted below, is not generally valid and it has no advantages over other alternatives.

A significant improvement in the problematic areas of the Smagorinsky model is made by the dynamic approach (dynamic Smagorinsky model). In this model, the constant C_s is given a *local* value that is derived by assuming an asymptotic behavior of the SGS term as the filter size is reduced. The approach is done by using two filters of different sizes in order to make an estimation of the SGS behavior and thereby obtaining an optimal C_s value. The dynamic approach can handle fully resolved regions by computing the vanishing value of the coefficient. Also, if the assumption of asymptotic behavior is valid for any reason near the wall, the approach is still valid. The main difficulty that may be encountered is that the coefficient attains a negative value, which may lead to numerical instability. Olsson (1998) show that this issue can be circumvented by satisfying a total dissipative condition.

3.2.2b. *Implicit LES.* When the filtered equation (3.8) is approximated by a discrete approximation its principal appearance is:

$$\frac{\partial \overline{u}}{\partial t} + \frac{\partial F(\overline{x})}{\partial x} = \mathcal{G} + T(\overline{u}, \Delta x, \Delta t). \tag{3.11}$$

In equation (3.11), T represents the truncation errors of the discretization scheme.

The role of the physical SGS and the contribution of the truncation errors are additive. In fact, if one does not have a clear distinction between the filter width and the numerical scale (i.e. these two scales vanish at the same rate), the effects of the SGS terms can hardly be distinguished from the effects of the discretization errors. This is so since, as the filter and numerical scales are

reduced, the contribution of the SGS and the discretization error terms become arbitrarily small.

A general problem is that one has to express the effects of SGS in terms of the resolved scales and the loss of information (due to filtering) has to be recovered. It is not self-evident that such a deconvolution is possible at all without introducing a set of assumptions. Therefore, when explicit SGS models are used, some hypothesis or physical reasoning must be introduced in order to resolve this.

Another important issue with SGS is near solid walls, where the small scale behavior is far from being universal (though the SGS term vanishes for small enough filter scale).

In the Large Eddy Simulations performed in this work, no explicit subgrid scale model is used (Grinstein *et al.* 2007), and we strive at using adequately fine grids so that the error caused by approximating the SGS terms are of the order of the truncation errors (i.e. the right hand side of of equation (3.11). For this approach the inherent dissipation of the numerical schemes is used to account for the dissipative role of the SGS term.

The advantages with this LES approach are simplicity and low computational cost. However, the dissipation of energy and any structural properties of the unresolved scales are completely dependent on the grid and the numerical scheme (i.e. non-physical parameters), making the identification of the SGS effects difficult. For conventional LES using a dissipative SGS model such as the Smagorinsky model, it is essential that the numerical dissipation is as low as possible so that the small scale effects are left to the model. For LES without explicit SGS model (i.e. the so called "implicit" LES), the coupled nature of the SGS effects and the numerics requires that the spatial resolution is adequate.

Generally speaking, using explicit SGS models allows one to use somewhat coarser grids. Finally, one might argue that implicit LES is not true LES as it will converge to a DNS if the resolution is increased. Because of this, one cannot obtain (in implicit LES), in the strict sense, grid-independent solutions except in the DNS limit. If this property is important or not is largely a question of preference as the usability, applicability and accuracy of the implicit LES approach has been demonstrated in many occasions and for a large number of different flow cases (Grinstein *et al.* 2007).

3.2.3. *Reynolds Averaged Navier-Stokes*

Reynolds Averaged Navier-Stokes is the most common way of dealing with turbulent flow computations, at least for engineering problems. This approach uses averaging of the instantaneous fields in the NSE to obtain an equation for the mean fields. Averaging is done by decomposing the instantaneous fields in the following way: $u_i \equiv U_i + u_i'$ and $p \equiv P + p'$ creating an average and a

fluctuating part. If this decomposition is applied to the incompressible NSE, the RANS equations are obtained as:

$$\frac{\partial U_i}{\partial x_i} = 0, \tag{3.12}$$

$$\frac{\partial U_i}{\partial t} + U_j \frac{\partial U_i}{\partial x_j} = \frac{1}{\rho}\frac{\partial P}{\partial x_i} + \frac{\partial}{\partial x_j}\left(2\nu S_{ij} - \overline{u_i' u_j'}\right). \tag{3.13}$$

In equation 3.13, $S_{ij} \equiv (U_{i,j} + U_{j,i})/2$, the mean strain rate tensor. The last term in the momentum equation (3.13), $\overline{u_i' u_j'}$, is called the Reynolds stress tensor and contain the additional stress on the mean field due to the turbulent fluctuations. The Reynolds stress must be modeled in order to close the RANS equations and there are many ways to do this which, in principle, can be categorized by the character of the model used for the Reynolds stresses.

The eddy viscosity assumption states that the turbulent stresses depend on local phenomena only, which can be a reasonable approximation in simple shear flow such as flat plate boundary layers, channel flow or mixing layers. In highly three-dimensional flows, or flows containing large-scale fluctuations such as separation bubbles, the assumption is not equally reasonable. Examples of models based on the eddy viscosity assumption include the Baldwin-Lomax and the Spalart-Almaras models, where the latter one is widely used in the aircraft industry. So called "complete models" using the eddy viscosity assumption are the most commonly used RANS models overall: The $k-\varepsilon$ and the $k-\omega$ models belong to this class.

Less commonly used in industrial applications are the Reynolds stress models, where the eddy viscosity assumption is replaced by a transport equation for the Reynolds stresses. This removes the assumption that the turbulent stresses are isotropic and dependent only on local quantities. The Reynolds stress models are in principle more general when compared to the eddy viscosity approach.

3.3. Computational aspects

For all the work presented here a general purpose, compressible flow, finite volume CFD code was used, see Eliasson (2001). The system of equations is hyperbolic (i.e. real characteristics) and can be integrated numerically in time. The discrete problem, as the continuous problem, requires specifying boundary conditions. The number of conditions that has to be given for the continuous problem depends on the number of ingoing characteristics into the domain of interest. In principle, the discrete problem requires the same number of conditions. Some augmentation that depends on the particular spatial discretization can be necessary.

3.3.1. *Temporal discretization*

Advancing the flow equations in time can be done in several ways but in principle it is either implicit or explicit.

When employing implicit time stepping, a steady state-like iterative procedure is performed in each time step allowing larger time steps than numerical stability would allow in the case of explicit time stepping. This may greatly reduce computational time for some problems, when compared to explicit time stepping, and is the most generally applicable approach of the two.

Explicit time stepping uses a Runge-Kutta-type procedure to directly advance the flow equations in time making each time step much cheaper with regard to computational time compared to implicit time stepping. Additionally, explicit methods lend themselves more easily to parallel computation. However, as the length of the time step is directly linked to numerical stability it may require small time steps. In LES, for physical reasons, one uses time steps such that the fluid particles do not move more than one cell in a time-step. This might lead to, when the computational grid varies largely, that one could end up using very small time steps.

In the computations performed in this work, explicit time stepping using a three-stage Runge-Kutta scheme of formally first order accuracy is used. The time step length was chosen so that a maximum Courant number of around 0.6 was attained. First order formal accuracy may seem rather poor but, as the total accuracy of the method depends on a combination of spatial and temporal discretization, and the time steps are smaller by about three orders of magnitude when compared to the spatial steps, the spatial discretization is in fact more significant for the total accuracy.

3.3.2. *Spatial discretization*

When using LES, high resolution and low dissipation in the spatial discretization is very important. Using a central-type scheme gives low numerical dissipation but unfortunately also unphysical dispersion phenomena and spurious oscillations which necessitates the use of some numerical fix, such as a high order filtering, to stabilize the numerical algorithm.

One way which is commonly used in compressible CFD codes is to add artificial, non-physical, dissipation in some form to the equations. In this work, a Jamesson-type artificial dissipation (Hirch 1990) is used together with a second order accurate central scheme producing the required characteristics while maintaining the formal accuracy of the underlying scheme. The numerical algorithm is then stabilized by an dissipation-like mechanism, damping unphysical growth of oscillations in the computational domain. This type of dissipation is based on a blend of second and fourth order differences. In practice, the

computational code employs a sensor that enables the fourth order dissipation to be switched of in the vicinity of shocks.

3.3.3. *Boundary conditions*

For the in-, and outflow boundaries, physics dictates by the theory of characteristics the amount of information that is allowed to be specified. More precisely, the amount of in-going characteristics at each boundary determines the number of required boundary conditions.

At a subsonic inlet boundary, four conditions have to be given. At a supersonic inlet five conditions have to be given. At a subsonic or supersonic outflow one and no boundary conditions, respectively, are specified.

For all calculations preformed in this work, a constant mass flow subsonic inlet condition was used together with a constant-pressure subsonic outlet and adiabatic no-slip walls. The code employs directly the total temperature, flow direction and desired mass flow. Within the code, the total pressure is adjusted so that the desired mass flow is obtained at the inlet. The outlet boundary condition is set to a constant static pressure which may vary with time as in the bump calculations.

3.3.4. *Mesh*

For all computed cases, structured grids are used. The mesh used for the bump and valve port cases are stretched at the inlet and outlet. This is done in order to reduce the reflection of pressure perturbations since they are not the subject of study and may adversely effect the numerical stability. In the bump mesh, stretching is used also in the wall normal direction using a stretch factor of 1.01.

3.3.5. *Numerical accuracy and result comparison*

Determining the numerical accuracy of the code and comparing results obtained by computations to experimental results are two ways of evaluating the validity of the computational results. While the investigation of numerical accuracy is fairly straightforward, comparisons of numerical and experimental results can be surprisingly difficult.

The problem is not in the actual comparison, but rather in addressing the same problem. Difficulty arises from the fact that experiments and simulations seldom have the same boundary conditions, both in terms of the domain geometry and, more often, in terms of the flow conditions at the inflow and outflow boundaries.

The literature contains a large number of experimental data but only very few of these include a detailed description of the set-up so as to allow one to set

boundary conditions that are accurate enough (in terms of mean and turbulent quantities). The situation is even more problematic for LES, where one need instantaneous data at the boundaries.

With this background it is obvious that if one wants to make a side-by-side comparison of simulations and experiments then, aside from correctly describing the physics involved, one must put a considerable effort into making sure the boundary conditions match each other if close agreement is to be expected.

In order to determine the validity of the present work, the numerical accuracy of the code has been evaluated by a method proposed by Celik (2005) and qualitative results were are compared to experimental results by Bron (2003) and Sigfrids (2003).

Due to both the difficulty in accurately reproducing the inlet and outlet conditions of the experiments and the apparent insensitivity of the main flow features to the incoming boundary layer, it was decided that simplified boundary conditions could be used. These consist, as stated in the above section, of a constant mass-flow inlet with a plug inlet profile and a constant static pressure outlet.

The main flow features are well captured by the simulation despite these simplifications while the exact shock position and other quantitative results are not. Since the motivation for the bump simulations was not to validate the experimental results but rather to investigate the code capabilities regarding transonic flow and enhance the understanding of the sensitivity of the flow, the used boundary conditions are adequate.

The numerical accuracy study of the code resulted in an apparent accuracy of the order of 1.98, a result which must be considered very good with a formally second order spatial discretization. We conclude by stating that the ability of the overall method to accurately handle transonic flow seem to be good.

CHAPTER 4

Results

In this chapter we describe shortly the results for two cases that have been considered in this thesis, namely the bump flow and a generic outlet port valve geometry. Transonic flow in a wind tunnel past a bump has been considered first. This problem has a rather simple geometry as compared to an IC-engine port, yet the flow exhibits many of the complexities found in the engine case. In both cases, LES is used to capture the transonic phenomena and unsteady flow field.

4.1. Transonic bump flow

For the simulations of transonic bump flow the geometry of a wind tunnel experiment by Sigfrids (2003) and Bron (2003) is used. To investigate acoustic effects two different tunnel lengths have been considered. These have the size of $1150x120x200$ mm and $950x120x200$ mm, respectively (length x height x width). The bump has a chord length of 190 mm and a maximum height of 11 mm. The coordinate system of the computational domain is set so that the positive x-axis is in the streamwise direction, the y-axis is in the cross-flow direction and the z-axis is normal to the bump side of the tunnel. The origin of the coordinate system is in the spanwise center of the tunnel, on the bump side of the tunnel, immediately in front of the bump.

4.1.1. *General flow observations*

Qualitative investigations of the flow field in the tunnel confirm the occurrence of several expected phenomena observed in the experimental investigations by Bron (2003) and Sigfrids (2003).

Under all conditions tested, a shock system is formed in the channel as well as a significant separation of the boundary layer. The shock system and separation appearance varies considerably in the range of pressure ratios tested, examples of the instantaneous flow field at several different outlet pressures are shown in figure (4.1). Upstream of the bump, the developing boundary layer is very thin and is further compressed on the bump upstream of the shock. Downstream of the separation reattachment point, the flow has subsonic velocity and there are rapidly growing boundary layers on the walls. Depending on

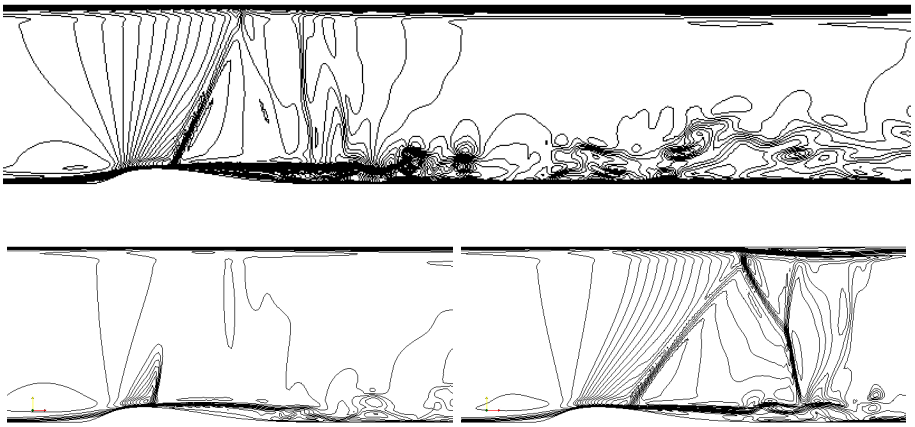

FIGURE 4.1. Instantaneous iso-Mach number lines at different outlet pressures. Top figure show an intermittently regular reflected shock. Bottom left figure show an unreflected shock. Bottom right figure show a Mach-reflected shock.

the tunnel pressure ratio, the shock is either regularly reflected, Mach reflected or not reflected in the tunnel ceiling, see figure (4.1). The shock and flow field

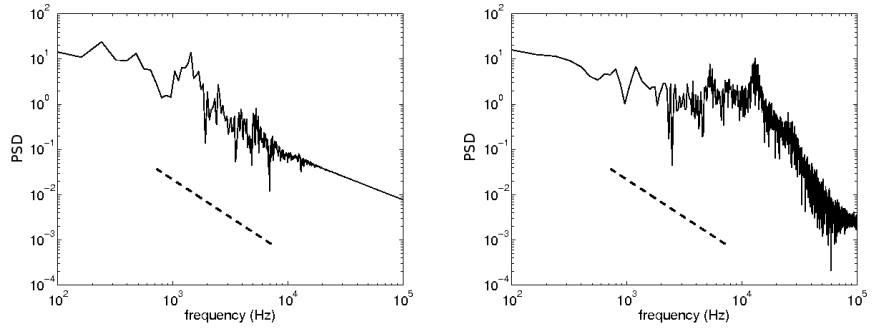

FIGURE 4.2. PSD of streamwise velocity fluctuation from the shock foot (left) and separation bubble.

downstream of the shock is unsteady in all the tested conditions. In figure (4.2) the PSD of the streamwise velocity fluctuations at two stations close to the bump surface can be observed. The left figure represent a point at the mean location of the shock foot, x_s while the data in the right figure is taken

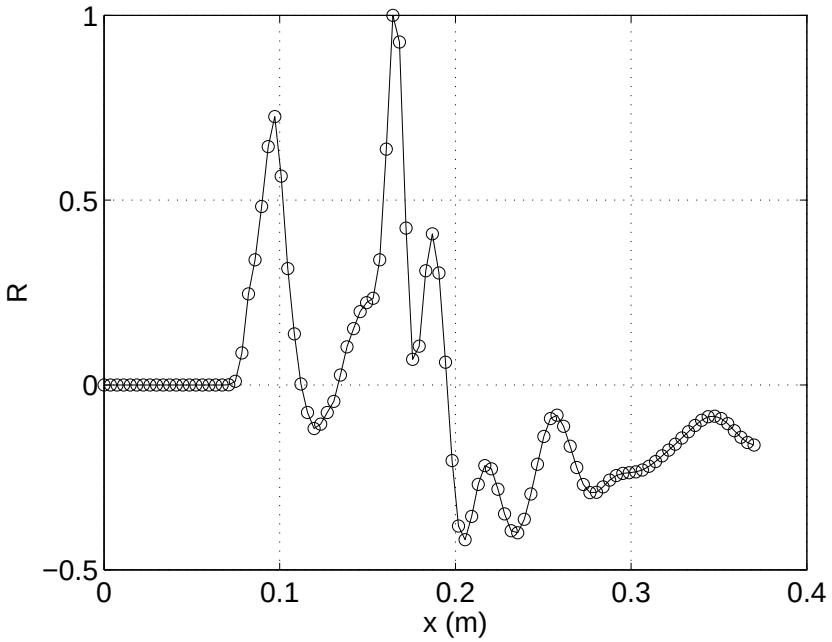

FIGURE 4.3. Spatial correlation of the streamwise velocity fluctuations along a line above the bump surface.

from the free shear layer of the separation at half the mean separation length, x_r.

No clear mutual peaks can be observed in the spectra of the two points but, as can be seen in figure(4.3), the velocity fluctuations are clearly related.

In order to investigate the interaction of the shock and the separated boundary layer the point x_r is used as a monitoring point. The auto-correlation of the axial velocity along a line 6 mm above the bump surface is correlated to the axial velocity at the monitoring point using:

$$R(x_r, x_m) = \frac{\overline{u_r(t)u_m(t)}}{\overline{u_m(t)^2}}, \tag{4.1}$$

where x_r and x_m represent two points along the line of interest. The results are plotted in Figure 4.3 where x_r is the point having $R = 1$. The peak having $R \approx 0.72$ is the physical location of the separation and shock foot, x_s. This result shows a strong spatial correlation between x_r and x_s implying that the unsteady motion of the shock foot and the separated boundary layer are strongly related.

The Strouhal number,

$$St = \frac{fL}{U}, \tag{4.2}$$

where f is the frequency, L a length and U a velocity is a useful tool. By forming the Strouhal number one may try to relate the peaks of the PSD of figure (4.2) to global velocity- and length scales and thus determine their origin.

The highest peak in the shock foot spectra at 1 kHz, left figure (4.2), is likely related to the global flow as it scales with the bump length and convection velocity. Also seen in this spectra is a harmonic of this peak, at 2 kHz. Moving on to the right figure (4.2) the dominant peaks are at 8 kHz and 10 kHz. The 8 kHz peak scale with the domain length and velocity of sound and is likely acoustic plane waves originating at the shock and then propagating up- and downstream in the channel. The 10 kHz peak can scale with the inlet flow velocity and bump height.

No direct evidence of the acoustic modes directly affecting the shock dynamics as mentioned by for example Sajben *et al.* (1984) could be found during this work. However, the behavior of the shock at high outlet pressures when the flow is not choked is significantly more unsteady compared to the choked flow. Acoustic modes are believed to be present in the channel at all outlet pressures, but when the flow is choked the disturbances emanating from the boundary layer dominates these and are the primary force behind the shock motion.

The proposed reason for the more unsteady and significantly different behavior observed is then that the acoustic modes contribute to the shock motion together with the boundary layer disturbances, when the flow is not choked. If they are of comparable strength, they may interact with each other and thus create a quite different perturbation profile compared to the case when the boundary layer disturbances dominate.

4.1.1a. *Forced flow oscillation.* To investigate the response of this sensitive flow to disturbances, periodic excitation at different frequencies was attempted. Excitation by means of varying both the outlet static pressure and the inlet mass flow was investigated, but only the former in a detailed fashion. The reason for this choice is that this is the preferred method of almost all prior investigations of transonic bump flow known to the author, making comparisons more straightforward. The outlet static pressure was varied within the limits of the steady boundary condition investigation in a sinusoidal fashion,

$$p_{out} = p_0 + 0.08 p_0 \sin(2\pi f t), \tag{4.3}$$

where p_0 was set to 100 kPa. The excitation frequency was set initially to 5 Hz, but also 10 Hz and 30 Hz was tested.

The position of the shock foot as a function of the outlet pressure can be seen in figure (4.4), together with mean positions from computations using steady boundary conditions. The shock position shows clear hysteresis for all forcing frequencies.

The shape of the shock position traces indicate the formation of a cycle where the shock position depends, for a given back pressure, on if the flow is accelerating or decelerating. When the perturbation frequency is varied the shape of the position trace also varies quite significantly. Comparing the three

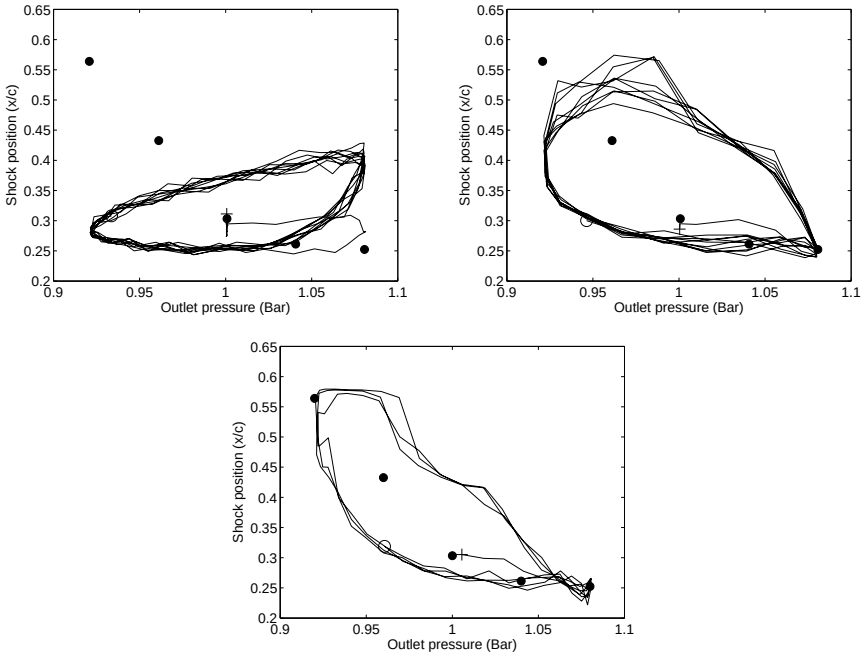

FIGURE 4.4. Position of the main shock as function of the varying outlet pressure. Top left: 30 Hz perturbation frequency. Top right: 10 Hz perturbation frequency. Bottom: 5 Hz perturbation frequency.

different plots in figure (4.4) one can see that the amplitude of the shock motion seems to decrease as perturbation frequency increases. For 5 and 10 Hz, the deviation from the steady BC data at an outlet pressure of 100 kPa is more significant when the flow is decelerating compared to accelerating flow. In the case of 30 Hz perturbation frequency, the deviation is more or less the same at this point. In general, the 30 Hz case stands out in comparison to the two

lower frequencies and must be quite far removed from the quasi-steady regime in which at least the 5 Hz case is located.

If some extrapolation is allowed from the presented data one could make the assumption that, if the perturbation frequency is very low, the trace would be on top of the steady BC data, and, if it was very high there would be no shock motion. In physical terms, the response time of the system is finite and not dependent on the forcing frequency as can clearly be seen in figure (4.4). If the perturbation frequency is very high, this response time will be too long for the shock system to adjust to the change in conditions leading to the decrease in amplitude which can be observed already at 30 Hz.

The reasoning behind the other perturbation frequency limit is that if the frequency is precisely zero, the flow has stationary boundaries. If the frequency is very low, the flow behavior is likely to be very close to the steady case.

There may however be perturbation frequencies at which the shock behavior deviates from this proposed behavior if resonance in the system occurs. The possibility of resonance exists if the natural oscillation frequency of the shock locks in to the perturbation frequency. The natural oscillation of the shock is quite broad-band and situated at frequencies an order of magnitude above the tested ones, explaining why no resonance has been observed.

Due to practical reasons the low frequency perturbation cases have a smaller amount of recorded periods compared to the high frequency ones. This means that the settling behavior of the position trace at different frequencies can not by evaluated equally and that especially the trace of the 5 Hz case, having only 3 periods of data, is difficult to analyze at all. So, the nature of the trace and the kind of attractor will not be discussed. To further analyze the data from the forced flow, the RMS of the static pressure along a line on the bump surface in the center of the channel was studied. The data in figure (4.5) show clearly the difference in the amplitude of the shock oscillation when comparing the different cases in the width of the first peak.

Another clear difference is the maximum of the RMS in the shock peak, and also the different appearance in the reattachment region. All the perturbed cases have a higher RMS at the shock location compared to the separation region while, for the steady BC case it is the opposite. That the RMS levels are much higher for the perturbed cases is quite natural as the amplitudes are naturally higher because of the perturbation.

In order to explain the hysteresis one must first consider a coordinate system in which the shock is at rest. In such a system the motion of the shock, which results from the change of pressure ratio over the domain, will cause a higher shock Mach number when the flow is decelerating and the shock moves upstream and a lower shock Mach number when the shock moves downstream

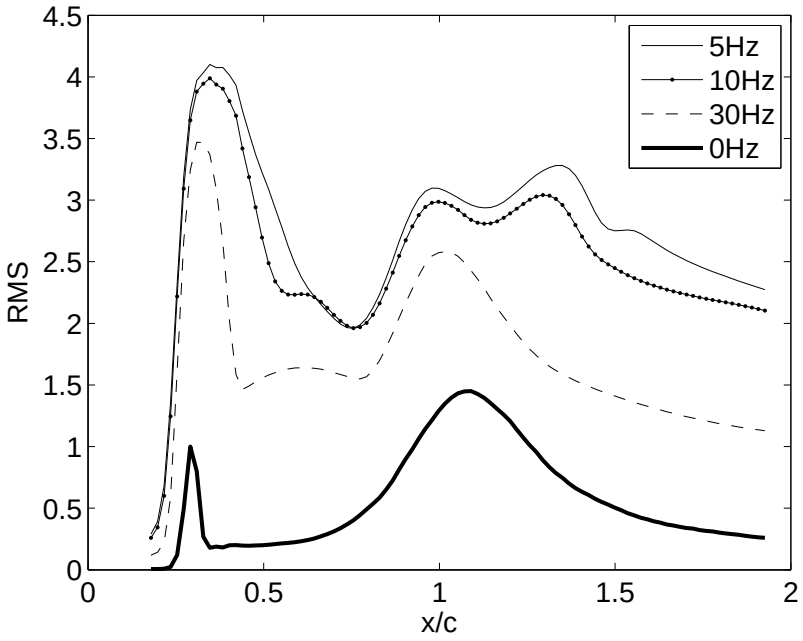

FIGURE 4.5. RMS of pressure on the bump surface at channel centerline. Normalized by RMS value with steady boundary conditions at shock location.

in accelerating flow. This is so because the incoming flow Mach number changes very little over the range of the outlet pressure variation.

This behavior was also observed by Bruce & Babinsky (2008) among others. Because of this behavior, the shock Mach number will depend on the outlet pressure history causing the shock to assume a more upstream position in accelerating flow and vice versa for decelerating flow, compared to steady boundary condition calculations at the same pressure ratio. This behavior also causes the variation in the shock induced separation discussed in paper (2). The separation is more violent in the decelerating flow because of the higher relative Mach number and hence, stronger shock, compared to both steady boundary condition conditions and accelerating flow.

The total pressure loss is related to shock strength but there are also other sources of viscous losses in the considered flow. The shock Mach number varies between approximately unity and 1.5 so there must be a clear variation in the losses associated with the shock as the outlet pressure varies, something which is evident in the data. The reason for the lack of hysteresis in the total

FIGURE 4.6. Simplified exhaust valve geometry, cut at symmetry plane.

pressure loss is either that the shock strength does not exhibit hysteresis or that the balance of the sources of pressure loss may change as the flow accelerates and decelerates. No attempt has been made to separate the different sources of loss but it is expected that the shock is dominant. Thus, the first suggestion above is the most likely.

4.1.2. *Summary*

The flow considered shows the expected general behavior when compared to both experiments and calculations of similar flows. The shock is unsteady in all conditions and the dynamics of the shock is strongly correlated to the unsteady separation. Hysteresis in the shock position was found when varying the outlet static pressure in a sinusoidal fashion at 5 , 10 and 30 Hz. The hysteresis occurs because of the varying shock Mach number in accelerating and decelerating flow at the same outlet pressure level.

4.2. Transonic flow in an model IC engine exhaust valve port

Simulations of the fluid flow in a model exhaust port, shown in figure (4.6), has been carried out. This model has dimensions comparable to those in a normal passenger car engine. Only one valve lift has been investigated and all geometries and boundary conditions are steady in time, meaning no moving piston or valve. Three different cylinder (inlet) pressures have been considered, as stated in table (1).

The justification for the simplification of stationary geometry is that compared to the flow velocity in the exhaust port, the valve velocity is an order of

magnitude less. The flow over the moving valve can then be viewed as several independent flows with different pressure ratios and valve lifts.

The boundary conditions are simplified for practical reasons, the correct *real* boundary conditions are not available for the geometry used and are not easily obtained. Actually, even if an actual engine geometry was used, the complete boundary conditions are not likely to be easily obtainable, if at all. If experimental data was available together with well documented experimental procedure, a much more physically accurate boundary description then what was used in this work is possible. Together with an actual geometry, it may then be possible to produce results with a more direct relevance to industrial geometries.

4.2.1. *Introduction*

High efficiency in the gas exchange process of an internal combustion engine is essential in order to construct engines with a high overall efficiency.

The exhaust part of the gas exchange process involves non-isothermal, turbulent, transonic flow in a non-trivial and non-stationary geometry. The flow around the exhaust valves contains unsteady supersonic regions and unsteady separation bubbles during the blow-down phase. When the exhaust valves open the pressure difference between the combustion chamber and the exhaust port is large, typically more than 50 bar. This, coupled with the small area connecting port and combustion chamber, may give rise to choking effects which limit the maximum mass flow through the valves.

The flow in the volume immediately after the exhaust valve can be characterized as three-dimensional, transonic and unsteady. The shape of the exhaust manifold leads to the formation of additional large unsteady flow structures. Furthermore, the acoustics in the manifold may have an environmental (noise) impact on the power-train system.

On the intake side of the gas exchange process, detailed knowledge of the flow field behavior is essential to ensure efficient combustion as the combustion process is highly dependent on the conditions in the cylinder prior to the actual combustion.

Some components of the inflow conditions do survive and others are amplified during the compression phase of the engine. For example, the swirl generated at the intake port survives and may be enhanced by the compression whereas the tumbling motion does not. This is the result of the instability of some modes and the stability of others as well as the change of geometry caused by the compression.

Because of such effects and their impact on fuel consumption and pollutant formation, much work has been done to understand the flow in the intake ports

and cylinder during the intake and combustion strokes both by the industry and in the academic world (Valentino *et al.* 1993; Bicen *et al.* 1986; Yasar *et al.* 2006; Lee *et al.* 2005).

More fundamental studies of the flow in the exhaust valve port are much less common, despite the impact of the flow on the turbo-charger and the after-treatment devices. Nevertheless, it has been shown (Ehrlich *et al.* 1997), that the flow into the turbocharger varies significantly during the engine cycle and that it contains flow structures that significantly affect the efficiency of the turbine. Another important issue is the loss of energy in the exhaust port associated with viscous phenomena and the importance of evacuating as much as possible of the exhaust gas before the end of the exhaust stroke.

Simple, mostly steady state flow and experimental, investigations involving the calculation of the discharge coefficient for a specific valve lift and exhaust port geometry with quite small pressure differences ($P_{in}/P_{out} \approx 1.1$) are carried out in the automotive industry.

These investigations typically focus on mean values of the losses for a specific geometry to determine the discharge coefficient and they do not consider the flow details at all. The data obtained in this way is often used in engine system simulation tools for the entire operational range of the engine. A more accurate description of the flow losses during the gas exchange, including a larger part of the engine operational range, may make these simulation tools more predictive than they are today.

Detailed investigation of the flow in the exhaust port by experimental methods is difficult due to geometrical constraints which makes it difficult to use measurement techniques such as hot-wire anemometry. On the other hand it is also difficult to gain optical access to the valve port region in order to use LDV or PIV measurement techniques. Therefore, it is essential to use numerical simulation in order to enhance the understanding of these flows. However, one cannot verify the numerical results directly in the primary regions of interest close to the valve due to the experimental difficulties and one must rely on data further up- and down-stream of the region of interest which may be more easily accessible for experimental investigations.

TABLE 1. Computed Cases setup for simplified geometry

	$P_{tot,in}(Bar)$	$P_{stat,out}(Bar)$
Case 1	3	2
Case 2	40	10
Case 3	120	2

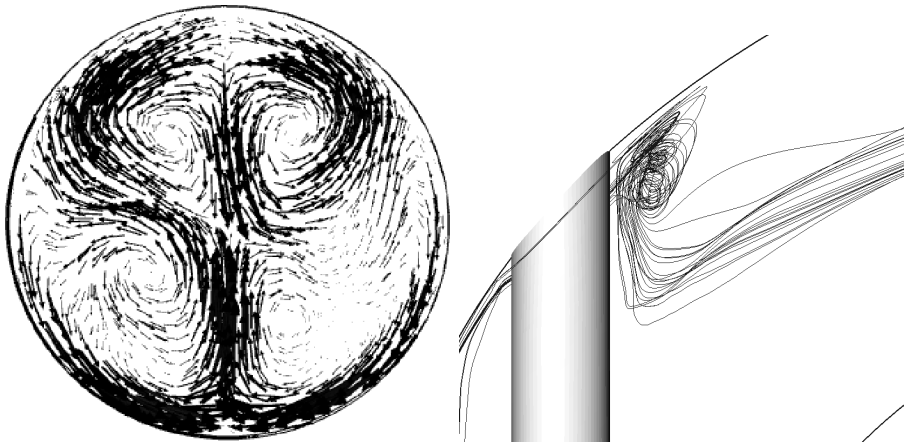

FIGURE 4.7. Left: Instantaneous in-plane velocity vectors one pipe diameter downstream of the valve. Arrows are in-plane velocity, axial flow is into the picture. Right: Streamlines showing the wake behind the valve.

4.2.2. *General flow observations*

The flow in the model exhaust port for the three cases are qualitatively similar to each other. At the inlet region, the flow is almost stationary at a high static pressure. Near the valve, the flow is rapidly accelerated to a high velocity (supersonic for Cases 2 and 3). After the valve plate, the geometry expands and makes an almost 90° turn while passing the valve stem. At the bend the flow velocity is significantly higher in the outer part. This is the most interesting part of the flow as it exhibits significant unsteady dynamics and is the birthplace of two pairs of counter-rotating vortices, one in the upper part and the other in the lower part of the port, shown in see figure (4.7).

These vortex pairs are formed by different mechanisms: The lower pair is created by inertial forces and the pressure gradient in the pipe bend while the upper pair is created by interaction between the wake behind the valve and the free stream.

The pressure gradient in the bend is directed inwards and the low-momentum fluid at the pipe walls are forced in this direction by this gradient. Inertial forces work in the opposite direction, outwards, and the result are the lower pair of vortices.

The wake behind the valve stem can be seen in figure (4.7), the low-momentum fluid in the wake exits downward in the picture due to the pressure gradient in the pipe. When this fluid interacts with the mean flow, from left to right in the figure, the two upper vortices are created.

4.2.3. *Spectral and correlation analysis*

In order to confirm the general observations made and also make some more quantitative analysis, the power spectral density (PSD) and autocorrelation techniques were used on data recorded along the centerline of the port channel. All data is obtained by first running the simulation for approximately 20 flow-through times and then gather statistics during 20 additional flow-through times. This procedure is used to ensure that the results are free of dependence on the initial conditions, to a reasonable degree.

The dominant peaks in all the spectra can be associated to the valve stem diameter and flow velocity by the Strouhal number. The likely origin of the peaks is the dynamics of the outer vortex pair because of the close connection to the valve stem by the Strouhal number, of order unity, of these peaks.

The correlation analysis show that the disturbances quickly dissipated out for cases 1 and 3, but survived for case 2. The cause for this may be that because case 2 never relaxes back to subsonic flow after the first acceleration the flow is supersonic in the downstream part of the exhaust port. This means that, although losses are higher in this case (even higher than case 3), there are no disturbances propagating upstream in the core flow who can disturb the structures created at the valve and in the bend. These disturbances may cause the created structures to dissipate faster for the two cases with subsonic flow in the downstream part of the port.

A more detailed analysis, together with figures can be found in paper (3).

4.2.4. *Summary*

The flow in the considered geometry was found to be highly unsteady, something which is expected also in industrial geometries. Vortex structures are formed in the bend, both by wake interaction, pressure gradients in the bend and inertial effects. The mechanisms responsible for the creation of the vortical structures observed in the flow are such that they can be expected to be present also in other port geometries. The generated structures stay more coherent during convection for case 2 compared to the other cases, possibly because of less disturbances in the flow field for this case. Total pressure loss was highest for case 2, the case with supersonic flow velocity at the outlet. For the two subsonic outflow cases losses were higher for case 3, which has higher flow velocity.

CHAPTER 5

Summary and future work

Large Eddy Simulations of the transonic flow past a bump and in a model IC engine exhaust valve port has been carried out.

The results from the first investigation show that a subsonic inflow is accelerated to supersonic velocity as it passes the bump for low enough outlet pressure where a shock system is formed, terminating the supersonic region. The formation of a shock lead to shock-induced separation of the incoming boundary layer due to the large pressure gradient over the shock. Primarily due to a strong coupling of the shock and separation dynamics, the shock system is always unsteady. The flow is highly sensitive, making small changes in the boundary conditions result in significant variations in the shape and type of shock system as well as separation appearance. The shock system position exhibit a hysteretic behavior when the outflow pressure was varied with a low frequency. This behavior is due to differences in relative shock speed in accelerating and decelerating flow.

The latter investigation show that at realistic pressure ratios in a model exhaust port, transonic flow is obtained. For all computed cases, two pairs of vortices are created in the exhaust port by interaction with the valve stem and by inertial effects and the pressure gradient in the pipe bend. The pairs are located in the top and bottom parts of the exhaust port, respectively. The upper vortices, originating in the interaction with the wake behind the valve stem is responsible for the main unsteadiness in the flow while the lower pair are low-momentum and thought to not be driving any unsteadiness. The spectral and correlation investigation confirm periodical motion originating in the wake interaction and show that the periodical structures quickly dissipate.

5.1. Future work

All the work presented here is preparatory for computations of actual exhaust port geometries. The intention is to build on the knowledge gained by this work and expand the study to moving, industrial geometries. As this study has shown, the flows considered are very sensitive to the boundary conditions, something which can also be said for LES or CFD in general. If one expects

accurate results, then one must pay very close attention to the boundary conditions used. One great challenge, at least at the present stage, is to obtain the correct boundary conditions for simulations of an industrial geometry. The aim of the future studies is to identify, and quantify, loss sources and flow structure-generating mechanisms in industrial geometries.

Acknowledgments

First of all I would to thank my supervisor Professor Laszlo Fuchs for all encouragement, support and guidance throughout this work.

I would also like to thank all the people at the department of Mechanics who I interact with every day, you make my days more interesting. I would especially like to thank Fredrik H for all the help and discussions, Ramis for dragging me around Berlin (and being nice in general) and Fredrik Lundell for the much appreciated comments on this thesis. Peter, Stefan, Simone and Oskar, thank you for all your help with EDGE.

The CICERO competence centre is greatly acknowledged for the financial support.

Last, but definitely not least, I would like to thank Fia and my family for love and support.

References

Anderson, J. 2003 *Modern compressible flow, third edition*. McGraw-Hill.

Ben-Dor, G. 1999 Hysteresis phenomena in shock wave reflections in steady flows. *Journal of Materials Processing Technology* **85**, 15–19.

Ben-Dor, G., Ivanov, M., Vasiliev, E. & Elperin, T. 2002 Hysteresis processes in the regular reflection mach reflection transition in steady flows. *Progress in aerospace sciences* **38**, 347–387.

Bicen, A. F., Vafidis, C. & Whitelaw, J. H. 1986 Steady and unsteady air flow through an intake valve of a reciprocating engine. *Tech. Rep.*. Department of Energy, Washington, DC. DOE/NBM-6005208.

Bogar, T., Sajben, M. & Kroutil, J. 1983 Characteristic frequencies of transonic diffuser flow oscillations. *AIAA Journal* **21, no 9**, 1232–1240.

Bron, O. 2003 Numerical and experimental study of the shock-boundary layer interaction in transonic unsteady flow. PhD thesis, Dept. Energy Technology, KTH.

Bruce, P. & Babinsky, H. 2008 Unsteady shock wave dynamics. *Journal of Fluid Mechanics* **603**, 463–473.

Celik, I. 2005 Procedure for estimation and reporting of dicretization errors in cfd applications. *Tech. Rep.*. Mechanical and Aerospace engineering department, West virginia university, Morgantown Wv, USA.

Chen, C., Sajben, M. & Kroutil, J. 1979 Shock-wave oscillations in a transonic diffuser flow. *AIAA Journal* **17, no 10**.

Délery, J. 1983 Experimental investigation of turbulence properties in transonic shock/boundary-layer interaction. *AIAA Journal* **21, no 2**, 180–185.

Ehrlich, D. A., Lawless, P. B. & Fleeter, S. 1997 Particle image velocimetry characterization of a turbocharger turbine inlet flow. *SAE Special Publications* **1258**, 121–127.

Eliasson, P. 2001 Edge, a navier-stokes solver for unstructured grids. *Tech. Rep.*. Computational Aerodynamics Department, Aeronautics Division, FOI.

Galli, A., Corbel, B. & Bur, R. 2005 Control of forced shock-wave oscillation and separated boudary layer interaction. *Aerospace Science and Technology* **9**, 653–660.

Grinstein, F., Margolin, L. & Rider, W. 2007 *Implicit Large Eddy Simulation: computing turbulent fluid dynamics*. Cambridge university press.

Hirch, C. 1990 *Numerical Computation of Internal and External Flows vol. 2*. Wiley-Interscience.

Hornung, H. & Robinson, M. 1982 Transition from regular to mach reflection of shock waves part 2. the steady flow criterion. *Journal of Fluid Mechanics* **123**, 155–164.

Hornung, H. & Taylor, J. 1982 Transition from regular to mach reflection of shock waves part 1. the effect of viscosity in the pseudosteady case. *Journal of Fluid Mechanics* **123**, 143–153.

Lee, K., Ryu, J., Lee, C. & Reitz, R. 2005 Effect of intake port geometry on the in-cylinder flow characteristics in a high speed di diesel engine. *International Journal of Automotive Technology* **6(1)**, 1.

Lee, L. L. 1969 A simple formula for the shock polar. *AIAA Journal* **7 no.5**, 985.

Liu, X. & Squire, L. C. 1988 An investigation of shock/boundary-layer interactions on curved surfaces at transonic speeds. *Journal of Fluid Mechanics* **187**, 467–487.

Moroianu, D., Caraeni, D. & Fuchs, L. 2005 Large eddy simulation of a shock boundary layer interaction in a transonic internal flow. AIAA-2005-0312.

Olsson, M. Fuchs, L. 1998 Large eddy simulation of a forced semi-confined circular impinging jet. *Physics of Fluids* **10**, 476–486.

Pope, S. 2000 *Turbulent flows*. Cambridge university press.

Sajben, M., Bogar, T. & Kroutil, J. 1984 Forced oscillation experiments in supercritical diffuser flows. *AIAA Journal* **22, no 4**, 465–474.

Salmon, J., Bogar, T. & Sajben, M. 1983 Laser doppler velocimeter measurements in unsteady, separated, transonic diffuser flows. *AIAA Journal* **21, no 12**, 1690–1697.

Sigfrids, T. 2003 Hot wire and piv studies of transonic turbulent wall-bounded flows. Lic thesis, Dept. Mechanics, KTH.

Valentino, G., Kaufman, D. & Farrell, P. 1993 Intake valve flow measurements using piv. Fuels and Lubricants Meeting and Exposition, SAE paper 932700.

Yasar, A., Sahin, B. & Akilli, H. A. 2006 Effect of inlet port on the flow in the cylinder of an internal combustion engine. *Journal of Mechanical Engineering Science* **220**, 73–82.